Available online at www.sciencedirect.com
ScienceDirect
Journal of Power Sources 173 (2007) 60–67
JOURNAL OF POWER SOURCES
www.elsevier.com/locate/jpowsour

Advanced measurement techniques to characterize thermo-mechanical aspects of solid oxide fuel cells

J. Malzbender *, R.W. Steinbrech

Forschungszentrum Jülich GmbH, IEF-2, 52425 Jülich, Germany

Received 11 June 2007; received in revised form 23 July 2007; accepted 29 July 2007
Available online 8 August 2007

Abstract

Advanced characterization methods have been used to analyze the thermo-mechanical behaviour of solid oxide fuel cells in a model stack. The primarily experimental work included contacting studies, sealing of a model stack, thermal and re-oxidation cycling. Also an attempt was made to correlate cell fracture in the stack with pore sizes determined from computer tomography. The contacting studies were carried out using pressure sensitive foils. The load to achieve full contact on anode and cathode side of the cell was assessed and applied in the subsequent model stack test. The stack experiment permitted a detailed analysis of stack compaction during sealing. During steady state operation thermal and re-oxidation cycling the changes in open cell voltage and acoustic emissions were monitored. Significant softening of the sealant material was observed at low temperatures. Heating in the thermal cycling loop of the stack appeared to be less critical than the cooling. Re-oxidation cycling led to significant damage if a critical re-oxidation time was exceeded. Microstructural studies permitted further insight into the re-oxidation mechanism. Finally, the maximum defect size in the cell was determined by computer tomography. A limit of maximum anode stress was estimated and the result correlated this with the failure strength observed during the model stack testing.

Keywords: SOFC; Stresses; Sealing; Thermal cycling; Reduction; Re-oxidation

1. Introduction

The basic principles of solid oxide fuel cells (SOFCs) have their origin in the high ionic conductivity of stabilized zirconia of elevated temperature, first observed more than a century ago by Nernst [1]. Today, with substantial advances in theoretical understanding and experimental realization, the SOFC is considered a highly efficient device to convert chemical fuels directly into electrical power. The electrical efficiency (∼50%) increases further when coupled with a gas turbine in a power plant. In particular, in the past decade SOFC development has made significant progress resulting in a tenfold increase of power density [2].

There are essentially two main concepts under development, the tubular and the planar design [2,3]. Concerning long term stability and demonstration of plant technology, the tubular concept is far more advanced, whereas the planar design offers higher volumetric and gravimetric power density [2]. The development of robust, mechanically reliable planar SOFC stacks with the complex multilayer composite arrangement of cells and interconnects still faces various problems. They are related to differences in high temperature behaviour of the involved materials and their partial lack of thermo-chemical and thermo-mechanical compatibility in the stack composite [3,4].

The planar SOFC can be treated as a multilayer composite which consists basically of three layers, anode, electrolyte and cathode, where in actual cell designs either interfacial functional layers are added or gradients in material properties are tailored [5]. Since the layers are bonded in the composite, any mismatch in thermal expansion of the materials results in the development of residual stresses which are reflected in the curvature of the cells. Additional stresses can also emanate from the final arrangement and fixation of the cells in the SOFC stack, typically utilised using rigid glass ceramic sealants [6,7], thermal gradients resulting from thermal cycling [8] or isothermal operation or reduction and re-oxidation processes [9,10]. These stresses should not exceed the strength of the materials [11,12]. Hence, whereas steady state operation of SOFC stacks is asso-

* Corresponding author.
E-mail address: j.malzbender@fz-juelich.de (J. Malzbender).

0378-7753/$ – see front matter © 2007 Elsevier B.V. All rights reserved.
doi:10.1016/j.jpowsour.2007.07.072

ciated with degradation due to chemical processes, thermal and re-oxidation cycling may result in fracture of sealant or cell and thereby cause fatal damage of the entire stack [9,13].

Standard SOFC cells of the Research Center Jülich (FZJ) comprise yttria-stabilised zirconia (YSZ) as electrolyte, porous Ni-YSZ cermet as anode and lanthanum–strontium–manganite (LSM) as cathode [14]. Typical operation temperatures are in the range between 600 and 1000 °C. In order to operate the SOFC in the lower temperature regime (700–800 °C) either thin YSZ electrolytes and/or oxides with higher ionic conductivity, e.g. CeO, Sc stabilized zirconia, are used. Recent progress in electrochemical performance has also been achieved with improved cathodes. Composite cathodes (LSM + YSZ) increase the number of electrochemically active sites for oxygen reduction (three phase boundaries of electrolyte/cathode/air) [15]. Also new cathode materials of (La,Sr)(Co,Fe)O3 composition (LSCF) reveal superior performance [16].

In planar design larger power units of SOFCs require stacking of the cells and their connection in serial mode with intermediate bipolar plates via contact layers. Moreover, the fixation of the cells and the sealing of anode and cathode compartment need appropriate material solutions [17]. Since a prerequisite of successful stack operation is the permanent physical contact of geometrically stable planar cells, the assembling of a stack using curved cells typically includes application of an external force normal to the cell surface either at room temperature or at high temperature. However, a recent investigation has shown that the room temperature curvature for a sealed cell is negligible if the curvature has been eliminated at high temperature before cell fixation by the sealant using a perpendicular load [18].

In order to gain better insight into the thermo-mechanics and associated failure processes of solid oxide fuel cells in a stack, aspects of assembling have been assessed using a model stack. The experiments were carried out under safety gas conditions and operation with in situ monitoring of mechanical stack load, displacement, temperature, open cell voltage and acoustic emission [19]. In addition the stack and cell failure under conditions of thermal and reduction/re-oxidation cycling was investigated. Finally, it is shown that computer tomography can be used to asses the failure relevant maximum defect sizes in the cells and hence to predict a limit of the fracture strength. The presented investigations permit further insight into the behaviour of SOFC stacks especially in combination with previous results on the deflection of planar solid oxide fuel cells during sealing and cooling of stacks that were based on simulation in combination with in situ observations [18].

2. Experimental

The tests were carried out with anode supported SOFCs of planar design. In the case of the model stack test, FZJ standard cells were used, which had a porous Ni-YSZ as anode substrate or anode current collector (ACC, thickness ∼1.5 mm) that supported a co-fired YSZ electrolyte (thickness ∼10 μm) on an intermediate ∼10 μm thick anode functional layer (AFL) of higher density. The cells possessed a ∼50 μm thick Lanthanum Strontium Manganite (LSM) cathode. The metallic components of the stack (interconnects, cell-frames) were manufactured from Crofer22APU a ferritic steel that is available from ThyssenKrupp. Details on the design of the stacks can be found in ref. [6].

The supplementary contact and tomography studies were carried out with half-cells (no cathode). A pressure sensitive foil (Pressurex, Sensor Products) was used to visualize the contact situation as a function of load. Assuming a dominant influence of the brittle YSZ-sublattice on anode failure, the tomography studies were only performed with half-cells after chemically removing the Ni-compound.

3. Results

Subsequently the results of the contacting studies, model stack experiment and computer tomography are sequentially presented.

3.1. Contacting studies

Successful operation of planar SOFC components in a stack relies to a large extent on reliable, durable contact between the cell electrodes and the interconnect material. For a two cell short stack of FZJ design the electrical contact on the air side between anode substrate (Ni-YSZ) and interconnect (ferritic steel) is provided by a Ni mesh. The cathode is contacted to the interconnect using a compliant contact paste of proprietary composition. The necessary optimum contact load needs to be evaluated to eliminate any potential initial lack of contact due to the thermal mismatch warpage of “planar” SOFC cells. Therefore studies have been carried out introducing with pressure sensitive foil as a quantitative measurements method.

In FZJ stacks the anode—interconnect contact is ensured by a Ni-mesh with a wire thickness of ∼0.65 mm. In the contact experiments a Ni-mesh (100 mm × 100 mm) with the same specification as in the SOFC stack was spot welded to a flat plate of interconnect steel. The Ni-mesh was then loaded under compression using a flat ceramic plate as reference. For testing the contact situation a pressure sensitive foil was arranged between Ni-mesh and ceramic plate, hence permitting observation of the number of contact points after the test.

The contact foil images reveal that a spot welded Ni-mesh requires a high mechanical load (∼600 N) for maximum contact (Fig. 1). Interestingly, the same result is obtained if the test is carried out with an additional SOFC half-cell between Ni-mesh and ceramic plate. Hence it appears that the load to eliminate the characteristic deflection of a (100 mm × 100 mm) anode supported cells is lower (∼500 N) and the relevant stack contacting load is defined by the load necessary to provide an optimum number of contact sites on the Ni-mesh.

Tests on the cathode side have been performed via contacting the half-cell directly to the interconnect. Essentially the same load result was obtained. Note that the addition of a compliant contact paste and the soft cathode material, both not used in the present study will lead to a compensation of any remaining deflection.

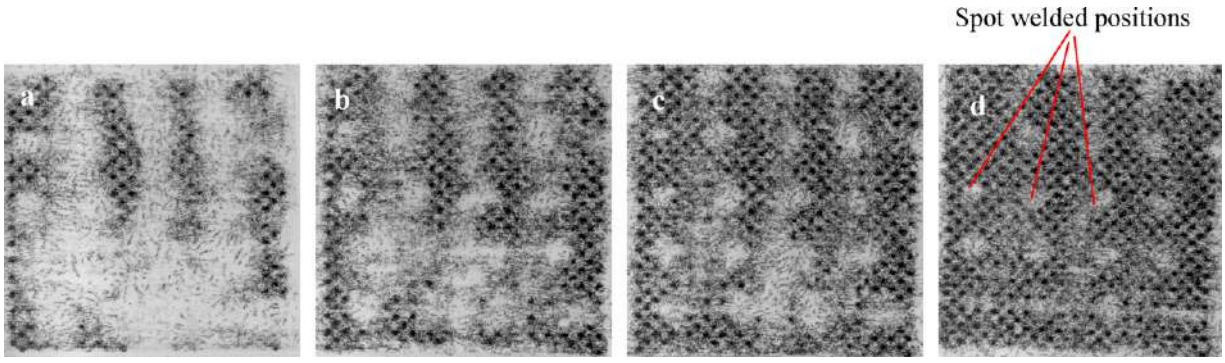

Fig. 1. Contact foil image after RT loading of a 100 mm × 100 mm Ni-mesh. Bright areas without contour reflect the situation of lacking contact. Sequence of increasing load demonstrates that lacking contact is finally limited to spot welded mesh positions: (a) 100 N, (b) 200 N, (c) 400 N and (d) 600 N.

Comparison of these experimental results with finite element simulations [18] suggests that a remaining cell deflection of ~1 μm is compensated by the Ni-mesh deformation. For both anode and cathode side a load of ~500 N is sufficient to provide maximum contact with a 100 mm × 100 mm cell of 1.5 mm thickness. This load was applied during the model stack test. The choice of a 500 N stack load for cell contacting is also supported by additional high temperature tests. The coarse Ni-mesh used in the stacks deforms predominantly elastic at room temperature (RT), however, at the stack sealing temperature of 850 °C plastic deformation dominates. In addition ~20 μm creep occurs within 24 h at 850 °C if the Ni-mesh is loaded with 500 N that might be considered in stack design.

3.2. Model stack experiment

A model stack experiment was carried out with a two-cell stack within the high temperature furnace of a mechanical testing machine. A schematic of the experimental set-up, which also illustrates the testing parameters, is displayed in Fig. 2. The experiment was instrumented for monitoring the mechanical stack load, the stack displacement (height reduction), temperature, open cell voltage and acoustic emission. In addition one side face of the stack was in situ observed using a high resolution CCD camera with magnifying lens system. A front view of the (still open) furnace in the mechanical testing machine with the stack centred between ceramic loading pistons is shown in Fig. 3.

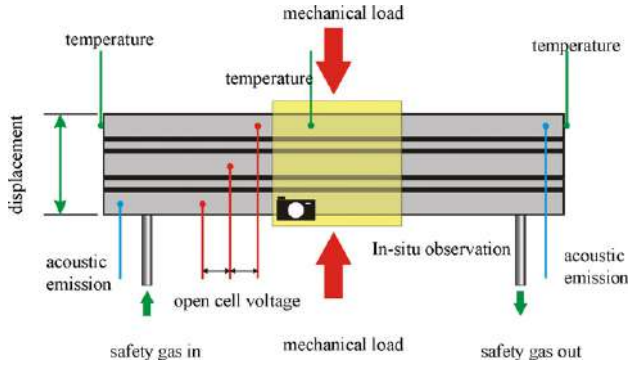

Fig. 2. Schematic of the experimental set-up before testing.

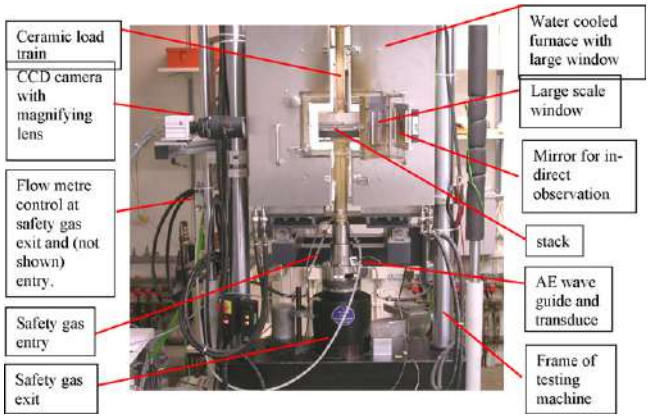

Fig. 3. Front view of the (still open) furnace in the mechanical testing machine with the stack centred between ceramic loading pistons.

The image also displays part of the instrumentation (acoustic emission: AE), the safety gas supply tubes and the CCD camera. The rear view of the stack before the experiment (Fig. 4) illustrates were temperature, OCV and AE were measured.

The testing sequence comprised in a first phase the assembling procedure (sealing) and, after crystallization of the glass ceramic sealant, the anode reduction with 4% H_2/Ar (safety gas). Thereafter multiple thermal heating–cooling loops with increasing temperature rate were performed. Re-oxidation and reduction cycles completed and terminated the experiment.

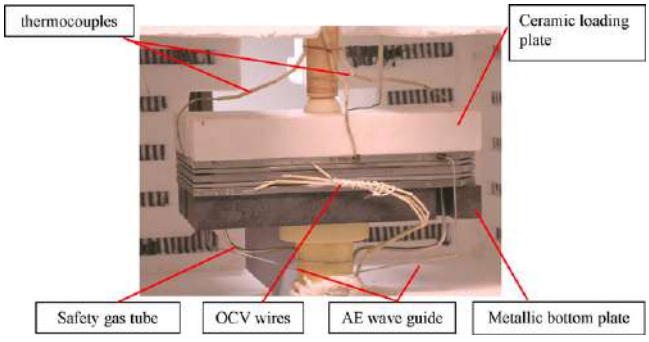

Fig. 4. Rear view of the stack before the experiment illustrating were temperature, OCV and AE were measured.

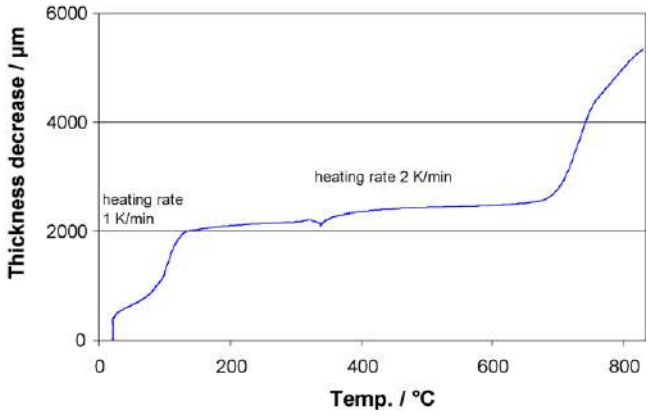

Fig. 5. Sealing of the model stack. Sealant shrinkage by deformation of glass ceramic paste at about 100 °C and softening above 700 °C.

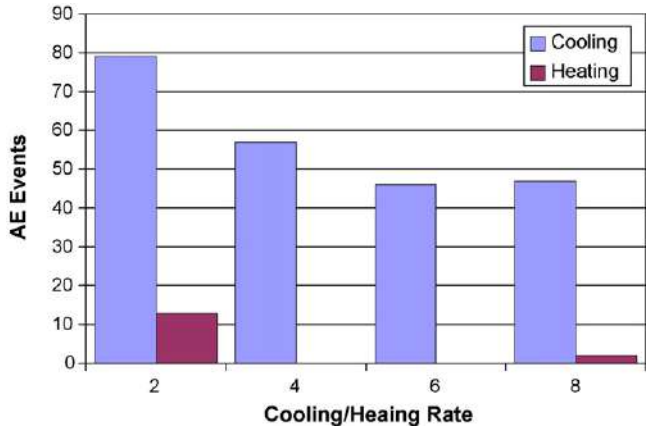

Fig. 7. AE events as a function of heating and cooling rates. Effect most pronounced during cooling.

3.2.1. Results related to the different testing stages

The experiment consisted of four stages. The initial sealing phase and anode reduction was followed by an operation period of ∼25 h at 800 °C. Then the stack was thermally cycled with heating rates of 2, 4 and 8 K min^{-1}. No variation of cooling was applied; hence the cooling rate was in each case identical with furnace cooling. During the thermal cycling test it was assumed that the stack reached the constant operation temperature of 800 °C when the open cell voltage had stabilized. After reaching this thermal equilibrium the cooling part of the thermal cycling was started. The final stage of the stack test focused on re-oxidation cycles. Experimentally, the safety gas supply was interrupted; no additional air feeding was introduced. Hence, the re-oxidation time depended on the leakage rate of the system.

3.2.2. Sealing

The change in thickness during the assembling procedure of the paste to be crystallized to a glass-ceramic and used for sealing the stack is illustrated in Fig. 5. Two significant upward changes of displacement are observed during the heating to 850 °C which correlate with a compaction of the stack height. The paste exhibits a first pronounced deformation at ∼100 °C (1) followed by softening above ∼700 °C (2). The shrinkage behaviour was also documented in a video sequence mounted from the images of the in situ CCD camera observation on the stack side face. Fig. 6 shows RT-micrographs of the sealant paste before the experiment, after annealing to 150 °C and in the crystallized state. After annealing to 150 °C the paste appears more compact and finally displays crystalline phases. The crystallization period of the seal (∼25 h, 800 °C) is accompanied by a slight increase in stack height of ∼100 μm. The crystallisation processes of the glass ceramic sealant are known to occur mainly during the first hundred hours and thereafter saturate [20,21].

3.2.3. Thermal cycling

During thermal cycling open cell voltage and acoustic emission signals were recorded simultaneously. Initially the open cell voltage was lower than expected due to short circuiting of OCV wires. Visual stack examination after a first cooling down revealed that OCV wires had gained accidentally contact with the wave guides of the AE sensors during the sealing procedure. The wiring was adjusted before the re-heating. Also a problem emanated from the common ground potential of the AE amplifiers since the wave guides for the AE sensors were welded to the upper and lower cell. Removal of one AE sensor resulted in a significant increase in voltage. Thus rather than measuring between bottom and top of the stack, the AE wave guides were connected to opposite sides of one stack plane only. After fixing the wiring problems the open cell voltage of both cells was close to 1.1 V and hence in the expected range for the SOFC stacks.

Due to the addressed wiring problems the first thermal cycle could not be analyzed. In the next cycles thereafter only a low number of acoustic emission events were detected, mainly from the centre of the stack, which appeared to be associated with changes in the gas feeding rate. The number of acoustic emission events during cooling was always significantly larger than during heating. The number of events did not show a dependence on the heating/cooling rate within the investigated range (up to 8 K min^{-1}, Fig. 7), it rather decreased with the number of cycles. AE activity mainly started at temperatures below 600 °C. With

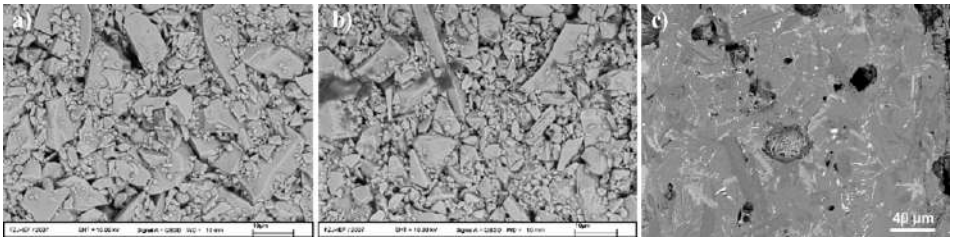

Fig. 6. Microstructure of glass-ceramic seal. (a) Glass paste at room temperature, (b) after annealing to 150 °C and (c) in crystallized state.

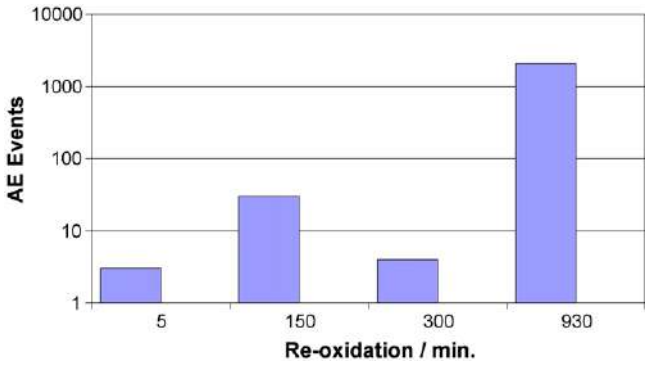

Fig. 8. AE events as a function of re-oxidation time. Effect most pronounced during cooling.

increasing number of cycles it was it was also possible to detect that most of the AE events preferentially occurred at the edges of the stack and hence were associated with fracture sources near or at the sealant location. It should be noted that a holding time of 65 h at room temperature led only to five AE events. Hence, there was no indication for slow environment (humidity) assisted crack growth under the stack conditions.

3.2.4. Reduction and re-oxidation

The AE activity was low during the reduction sequences. During re-oxidation the number of acoustic emission events increased strongly after some time. In Fig. 8 the rise of AE signals starts ~5 h from closure of the safety gas supply (gas outlet closed by flowmetre). Since the leakage of the complete stack system was not quantified, the given time frame has to be taken as being relative. However, the result is in agreement with previous microscopic observations of a re-oxidation front, which propagates (depending on oxygen supply) through the SOFC anode [9,13,22]. In the present experimental stack situation the number of AE events and hence the damage appeared to increase proportional to the time. Taking the thermal cycling history of the present stack into account a time of 5 h at 800 °C without safety gas was obviously sufficient to cause significant damage in the cells.

3.2.5. Post mortem inspection

The in situ monitoring of the AE activity from the stack test revealed fracture sources in the cells near the glass-ceramic sealant. Dismantling of the stack planes proved a very good bonding behaviour of the glass-ceramic. The dismantling fracture occurred essentially in the sealant [20,21]. Also a stronger bonding was recognized in case of thinner sealant, which was the case in the anode compartment. Both cells contained cracks, which were predominantly located along and near the glass-ceramic seals. The cracks were larger in the anode substrate (Fig. 9(a)), but could also be detected in the electrolyte (Fig. 9(b)).

3.3. Microstructural changes during re-oxidation

In order to further elaborate the significant anode and electrolyte damage observed after dismantling of the model stack. The microstructural changes within the sequence of NiO reduction and Ni re-oxidation were studied in supplementary laboratory experiments. Fig. 10 displays in a sequence of SEM micrographs with focus on exactly the same location the microstructural changes of an anode supported FZJ half-cell. The sequence from co-fired to the re-re-reduced state is displayed. The initially dense Ni-O particles (Fig. 10(a)) reveal shrinkage on reduction (Fig. 10(b)). The particles are fragmented in the re-oxidized state (Fig. 10(c)). Furthermore, electrolyte fracture and microcracks in the anode are visible. Reducing the NiO results again in dense particles (Fig. 10(d)) which appear to occupy a larger volume than in the initial reduced state (Fig. 10(b)), hence a courser structure. In the re-re-oxidised state the NiO particles appear to be even more fragmented (Fig. 10(e)). The electrolyte crack exhibits a larger opening. A reduction of the NiO with an additional holding time of 100 h (Fig. 10(f)) results in a similar structure as in the re-reduced case (Fig. 10(d)). Comparing the re-oxidized and the re-re-oxidized structure in Fig. 10(g and h) shows that in addition to crack opening the number of electrolyte cracks has increased. The increase of electrolyte damage in the re-re-oxidised state might be a result of the courser structure of the Ni in the re-reduced state. Complementary TEM investigations (Fig. 11) indicate that re-oxidation results in an increase of porosity in the NiO particles and that re-reduced and reduced structure look similar, however, some pores exist in the Ni particles.

Obviously the reduction step of Ni is not reversible by a subsequent re-oxidation. Compared to the initial state the porous re-oxidized NiO is more porous and hence requires a larger volume, causing compressive stresses in the anode and tension in the electrolyte. A ~0.5% strain increase compared to the initial

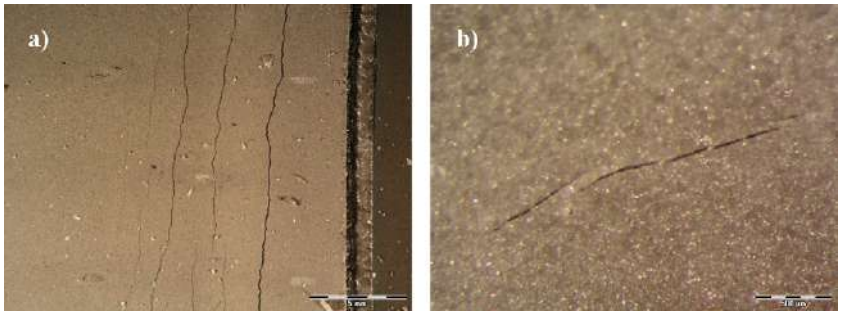

Fig. 9. Cell damage due to reduction/re-oxidation cycles. (a) Cracks in the anode and (b) electrolyte.

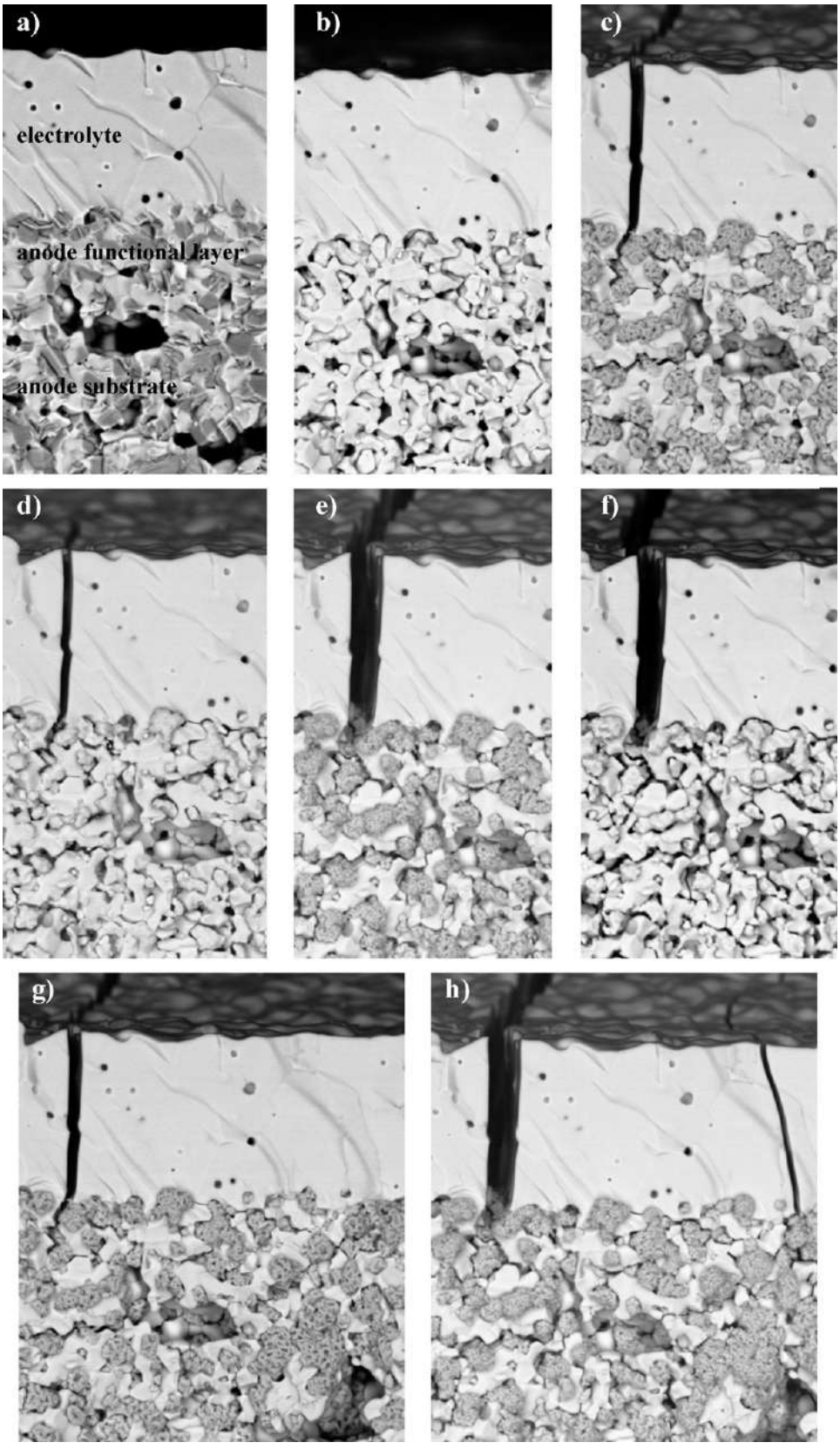

Fig. 10. SEM study of microstructural changes in anode and anode substrate due to reduction/re-oxidation cycles. (a) Initial as co-fired state, (b) reduced, (c) re-oxidized, (d) re-reduced, (e) re-re-oxidized, (f) re-re-reduced with additional holding time of 100 h, (g) re-oxidized and (h) re-re-oxidized.

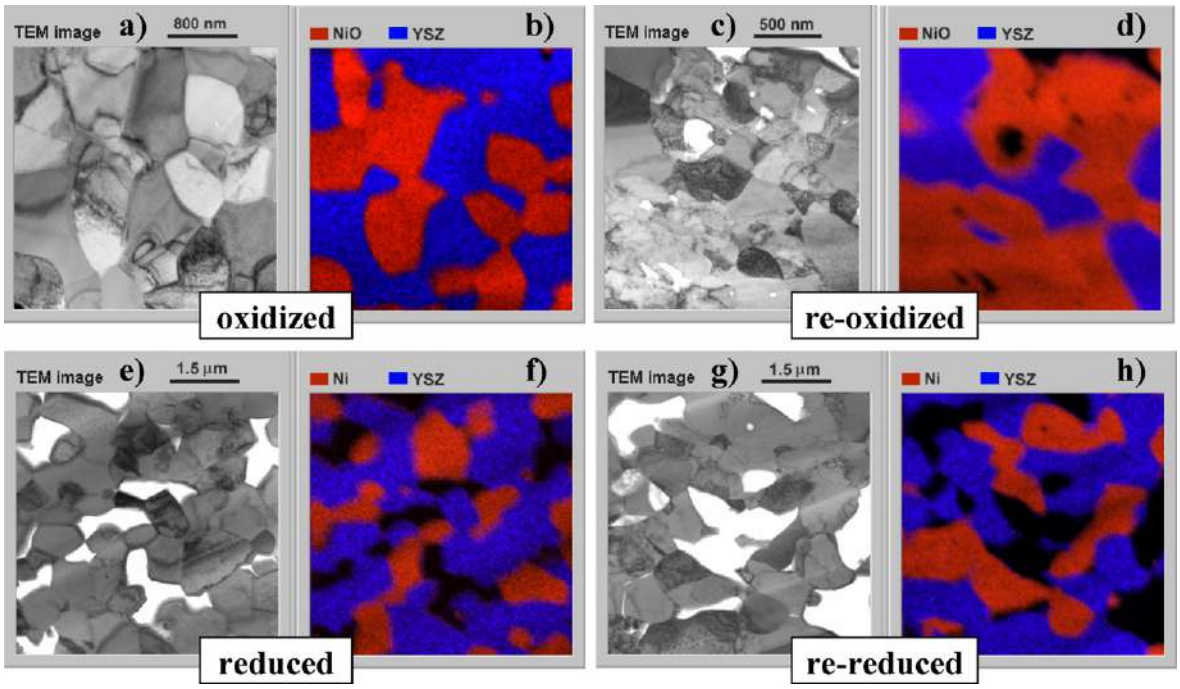

Fig. 11. Microstructural changes in anode and anode substrate. TEM micrographs of specimen prepared with Focused Ion Beam (FIB). (a and b) Co-firing, (c and d) re-oxidized, (e and f) reduced, (g and h) re-reduced.

oxidised state has been measured which is responsible for the electrolyte damage observed after the model stack re-oxidation experiments [9].

In addition to electrolyte cracks, cracks in the anode substrate have been observed after dismantling the model stack. These cracks might be a result of the in-plane additional oxidation front from the uncovered sides of the cell, whereas the electrolyte cracks can be associated with the perpendicular oxidation front from the free surface of the anode towards the electrolyte.

3.4. X-ray computer tomography

The multilayered, essentially brittle ceramic materials of the SOFC makes the composite component prone to brittle failure under the thermo-mechanical conditions of transient stack operation [11]. The model stack experiment described above give further proof of evidence. It is the defect population of the porous anode substrate which governs the possible fracture processes in anode supported planar SOFCs [11,18]. Thus an attempt was made to characterize the anode defects by a non-destructive method using computer tomography (CT) [23,24]. In cells with oxidised and reduced anode in the presence of NiO or Ni only the cutting damage was visible in the CT images.

In a half-cell specimen with reduced anode (Fig. 12(a)) pores which are considered to be the failure relevant structure related defects were only recognized after chemical removal of the Ni. The maximum observed defect size was ~400 μm, the minimum detectable defects were in the order of ~50 μm (Fig. 12(b)). No distinction could be made between the size of surface and volume defects.

Based on a fracture toughness value of ~1.2 MPa $m^{1/2}$ [20] for oxidized and reduced anodes the maximum defect size permits an estimation of a fracture stress made of ~50 MPa, which is within the range of strength values measured for FZJ cells using bending fracture methods [11]. The anode fracture observed as a result of the model stack re-oxidation can be associated with this stress level.

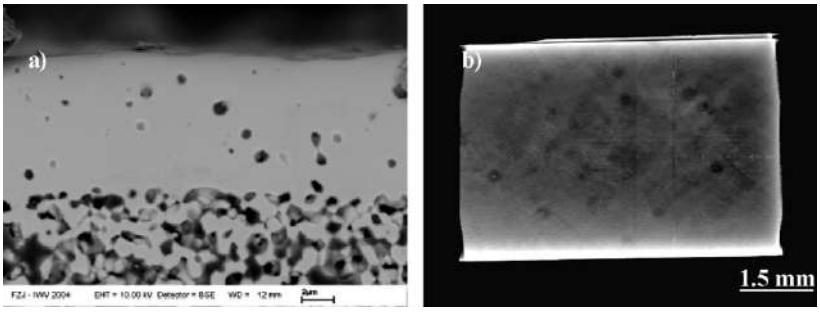

Fig. 12. SEM image of electrolyte and remaining YSZ frame (a) and cell section image obtained using computer tomography (b). The Ni has been removed chemically.

4. Conclusions

Contacting studies have been carried out. Pressure sensitive foil has been used to assess the necessary load for achieving full contact on anode and cathode side of the cell. A load of ∼500 N appeared to be sufficient to satisfy the demand. Note that also a remaining cell deflection of ∼1 μm would be compensated by local deformation of the contact materials.

The model stack experiment permitted a first analysis of the changes in stack height during sealing process. The in situ monitoring of acoustic emissions during steady state operation, thermal and re-oxidation cycling provide valuable information on mechanical stack failure mechanisms. A two-sensor acoustic emission method also proved to be a useful tool to assess localisation of damage.

Finally it should be emphasized that within the experimentally possible variation of the thermal cycling parameters the stack appeared to be insensitive to the heating/cooling rate, however, heating was in general less critical than cooling.

The computer tomography permitted an assessment of the maximum defect size. A strength value reasonable for FZJ cells could be estimated.

Acknowledgement

The work was partly supported by the EU under the project "Realising Reliable, Durable, Energy Efficient and Cost Effective SOFC Systems" (Real-SOFC). The authors would like to thank Dr. U. Reisgen for the computer tomographic measurement and Dr. P. Batfalsky for the help with post mortem inspection of the stack after operation. Furthermore, we would like to express our gratitude to Dr. E. Wessel for the SEM and Ms. D. Esser and Dr. J. Penkalla for the TEM investigation.

References

[1] W. Nernst, Über die Elektrolytische Leitung fester Körper bei sehr hohen Temperaturen, Z. Elektrochem. 6 (1899) 41–43.
[2] L. Blum, W.A. Meulenberg, H. Nabielek, R. Steinberger-Wilckens, Worldwide SOFC technology overview and benchmark, Int. J. Appl. Ceram. Technol. 2 (2005) 482.
[3] S.C. Singhal, Solid State Ionics 135 (2000) 305.
[4] O. Yamamoto, Electrochim. Acta 45 (2000) 2423.
[5] F. Tietz, H.-P. Buchkremer, D. Stöver, Solid State Ionics 152–153 (2002) 373.
[6] P. Batfalsky, V.A.C. Haanappel, J. Malzbender, N.H. Menzler, V. Shemet, I.C. Vinke, R.W. Steinbrech, J. Power Sources 155 (2006) 128.
[7] K.L. Ley, M. Krumpelt, R. Kumar, J.H. Meiser, J. Bloom, J. Mater. Res. 11 (1996) 1489.
[8] S.C. Singhal, K. Kendall, in: S.C. Singhal, K. Kendall (Eds.), High Temperature Solid Oxide Fuel Cells: Fundamentals, Design and Applications, Elsevier Ltd., Oxford, 2003, pp. 1–22.
[9] A. Atkinson, Solid State Ionics 95 (1997) 249.
[10] J. Malzbender, E. Wessel, R.W. Steinbrech, Solid State Ionics 176 (2005) 2201.
[11] J. Malzbender, R.W. Steinbrech, L. Singheiser, Ceram. Eng. Sci. Proc. 26 (4) (2005) 293.
[12] J. Malzbender, R.W. Steinbrech, J. Eur. Ceram. Soc. 27 (2007) 2597.
[13] M. Ettler, G. Blass, N.H. Menzler, Proceedings of the 7th European SOFC Forum, 2006, p. P0705.
[14] R.N. Basu, G. Blass, H.-P. Buchkremer, D. Stöver, F. Tietz, E. Wessel, I.C. Vinke, Simplified processing of anode-supported thin film planar solid oxide fuel cells, J. Eur. Ceram. Soc. 25 (2005) 463–471.
[15] V.A.C. Haanappel, J. Mertens, D. Rutenbeck, C. Tropartz, W. Herzhof, D. Sebold, F. Tietz, Optimisation of processing and microstructural parameters of LSM cathodes to improve the electrochemical performance of anode-supported SOFCs, J. Power Sources 141 (2005) 216–226.
[16] F. Tietz, V.A.C. Haanappel, A. Mai, J. Mertens, D. Stöver, Performance of LSCF cathodes in cell tests, J. Power Sources 156 (2006) 20–22.
[17] J.W. Fergus, Sealants for solid oxide fuel cells, J. Power Sources 147 (2005) 46–57.
[18] J. Malzbender, T. Wakui, R.W. Steinbrech, Fuel Cell 6 (2006) 123.
[19] K. Sato, H. Omura, T. Hashida, K. Yashiro, T. Kawada, J. Testing Eval. 34 (2006) 246.
[20] J. Malzbender, R.W. Steinbrech, L. Singheiser, J. Mater. Res. 18 (2003) 929.
[21] J. Malzbender, R.W. Steinbrech, P. Batfalsky, Ceram. Eng. Sci. Proc. 26 (4) (2005) 285.
[22] T. Klemensø, C. Chung, P.H. Larsen, M. Mogensen, J. Electrochem. Soc. 152 (2005) A2186–A2192.
[23] N.H. Menzler, P. Batfalsky, L. Blum, M. Bram, S.M. Gross, V.A.C. Haanappel, J. Malzbender, V. Shemet, R.W. Steinbrech, I. Vinke, Proceedings of the 7th European SOFC Forum, 2006, p. B104.
[24] S. Griesser, G. Buchinger, T. Raab, D.P. Classen, D. Meissner, Trans. ASME 4 (2005) 84.